Highly Conductive Ionic Liquid Electrolytes for Potassium-Ion Batteries

Takayuki Yamamoto,* Ryohei Matsubara and Toshiyuki Nohira

Institute of Advanced Energy, Kyoto University, Uji 611-0011, Japan

ABSTRACT

Potassium-ion batteries (K-ion batteries; KIBs) are attractive as high-voltage, low-cost energy storage devices. Ionic liquids (ILs) are potential candidates as safe and high-performance electrolytes for large-scale devices. Imidazolium-based ILs are known to possess high ionic conductivities and moderate electrochemical stabilities. In this study, we report the physicochemical and electrochemical properties of K[FSA]–[C_2C_1im][FSA] (FSA = bis(fluorosulfonyl)amide, C_2C_1im = 1-ethyl-3-methylimidazolium) ILs as new electrolytes for KIBs. A phase diagram constructed from differential scanning calorimetry results indicates that the melting point of this IL is below 273 K at compositions of x(K[FSA]) = 0–0.20 (x(K[FSA]) = molar fraction of K[FSA]). The viscosity, ionic conductivity, and density of the IL were measured for x(K[FSA]) = 0–0.20. The ionic conductivity at x(K[FSA]) = 0.20 is 10.1 mS cm^{-1} at 298 K, which is comparable to that of typical organic solvent-based KIB electrolytes and higher than that of other ionic liquid electrolytes for KIBs. The electrochemical stability of M[FSA]–[C_2C_1im][FSA] (x(M[FSA]) = 0.20; M = K, Na, Li) ILs was determined by cyclic voltammetry measurements. The K-based IL exhibits the widest electrochemical window of 5.19 V due to the negative redox potential of the K^+/K couple. Thus, the K[FSA]–[C_2C_1im][FSA] ionic liquid is expected to be a highly conductive KIB electrolyte.

1. INTRODUCTION

Ionic liquids (ILs) possess intriguing properties including non-flammability, superior electrochemical and thermal stability, and moderate ionic conductivity. Over the past several decades, they have been used as electrolytes in energy storage devices such as lithium-ion batteries (Li-ion batteries; LIBs) and sodium-ion batteries (Na-ion batteries; NIBs).[1–3] Although NIBs have advantages of low cost and abundant resources over LIBs, the maximum operating voltages of NIBs are intrinsically lower than those of LIBs due to the electrochemical windows of electrolytes. Since the operating voltage of battery cannot exceed the electrochemical window of electrolyte, the maximum operating voltage is determined by the electrochemical window. In general, the reductive stabilities of NIB- and LIB-electrolytes are determined by the redox potentials of alkali metals, and the redox potentials of Na^+/Na couple are more positive than those of Li^+/Li.[4] On the other hand, their oxidative stabilities are almost identical when the constituent ions or solvents are similar in the electrolytes. Thus, the electrochemical windows of Na-based electrolytes are narrower than those of the Li-based counterparts, resulting in the lower maximum operating voltages of NIBs. In other words, the redox potentials of alkali metals are one of the most important factors that determines the maximum operating voltages of batteries.[4] Recently, potassium-ion batteries (K-ion batteries; KIBs) have attracted attention as advantageous alternatives to LIBs, because potassium is plentiful in the Earth's crust,[5,6] and the operating voltage of KIBs is expected to be high. It is well known that, in the aqueous solutions, the redox potential of the K^+/K couple is more positive than that of Li^+/Li by 0.10 V and more negative than that of Na^+/Na by 0.33 V.[7] However, redox potentials depend on the type of electrolyte used. For example, the K^+/K potential in propylene carbonate (PC) solution has been predicted[7] and experimentally confirmed[5] to be more negative than that of Li^+/Li by approximately 0.1 V. One of the authors has investigated the

electrochemical properties of the ternary molten alkali TFSA salts, Li[TFSA]–K[TFSA]–Cs[TFSA] (TFSA = bis(trifluoromethylsulfonyl)amide).[8] Since the cathodic limit of the melt was confirmed to be the electrodeposition of lithium metal, the redox potential of the K^+/K couple is more negative than that of Li^+/Li.

Based on these backgrounds, we have focused on KIBs using IL electrolytes.[4,9–11] We have developed K[FSA]–[C_3C_1pyrr][FSA] (FSA = bis(fluorosulfonyl)amide, C_3C_1pyrr = *N*-methyl-*N*-propylpyrrolidinium) as a KIB electrolyte and compared the electrolyte properties among M[FSA]–[C_3C_1pyrr][FSA] (M = K, Na, Li).[9] The K^+/K potential in this environment is more negative than that of Na^+/Na by 0.35 V and that of Li^+/Li by 0.25 V, which is an advantage in developing batteries with higher operating voltages. However, K[FSA]–[C_3C_1pyrr][FSA], which has a K^+ concentration, $C(K^+)$, of 0.98 mol dm^{-3} at a K[FSA] molar fraction of x(K[FSA]) = 0.20, exhibits an ionic conductivity of only 4.8 mS cm^{-1} at 298 K.[9] Typical organic solvent-based KIB electrolytes with $C(K^+)$ = 1 mol dm^{-3} show ionic conductivities of approximately 10 mS cm^{-1} at 298 K.[5,6] Thus, development of a more conductive IL electrolyte is desirable.

Herein, we explore the use of imidazolium-based K[FSA]–[C_2C_1im][FSA] (C_2C_1im = 1-ethyl-3-methylimidazolium) ILs as KIB electrolytes. [C_2C_1im][FSA] has been used as an IL electrolyte in LIBs[12–15] and NIBs[16,17], but not in KIBs. The present work reports a systematic evaluation of the physicochemical and electrochemical properties of viscosity, ionic conductivity, density, and electrochemical window of K[FSA]–[C_2C_1im][FSA] ionic liquids.

2. EXPERIMENTAL SECTION

The alkali metal salts (M[FSA]; M = K, Na, Li) and [C_2C_1im][FSA] were studied under a dry argon atmosphere. K[FSA] and Na[FSA] were supplied by Nippon Shokubai Co., Ltd. Li[FSA] and [C_2C_1im][FSA] were purchased from Kishida Chemical Co., Ltd. and Kanto Chemical Co.,

Inc., respectively. The salts and ILs were dried at 333 K for 24 h prior to use. The water content was determined to be less than 50 ppm by Karl Fisher titration. M[FSA]–[C_2C_1im][FSA] (M = K, Na, Li) ILs were prepared by mixing the two salts in an argon-filled glove box. Chemical reagents used in this study are summarized in Table 1. It should be noted that the ionic liquid electrolytes with the compositions of $0.30 \leq x(\mathrm{K[FSA]}) \leq 0.90$ were prepared by mixing the K[FSA] salt and the [C_3C_1pyrr][FSA] liquid, and by heating up to around 373 K for more than 1 day to make homogeneous liquids. At this moment, no K[FSA] salts were remained visually. However, for all the liquids with the compositions of $0.30 \leq x(\mathrm{K[FSA]}) \leq 0.90$, the precipitates appeared after cooling to room temperature (~298 K).

Thermal behavior was investigated by differential scanning calorimeter (DSC; DSC8230, Rigaku Co.). Indium metal was used as a reference material for the DSC. To fabricate the cells for DSC measurements, the samples were heated to around 373 K to make homogeneous liquids again. After the precipitates completely disappeared, small amounts of the samples were immediately moved into the aluminum pan before solidification. Then, the pan is sealed using the aluminum lid to make air-tight cell. All the manipulations were conducted in the argon-filled glovebox. Viscosities (η) were determined using an electromagnetically spinning viscometer (EMS-1000, Kyoto Electronics Manufacturing Co., Ltd.) between 273 and 388 K at intervals of 5 K. A reference material for the viscometer was a standard liquid (JIS100) that conforms to JIS Z 8809 viscometer calibration fluid standard. Ionic conductivities (σ) were determined by AC impedance spectroscopy. The AC impedance spectroscopy were conducted within the frequency range of 50 kHz–1000 Hz using a T-shaped PTFE cell. Then, a part of the obtained plots was extrapolated with a straight line to real axis of the Nyquist diagram, and the crossing point was determined to be the resistance of the bulk electrolyte. The cell constant was calculated from the σ values of a

standard 0.1 mol dm^{-3} KCl aqueous solution. Density (ρ) measurements were conducted using a vibration-type density meter (DA-650, Kyoto Electronics Manufacturing Co., Ltd.) between 273 and 368 K at intervals of 5 K. Purified water was used as a reference material for the density meter. Viscosity and ionic conductivity plots were fitted with Vogel–Tammann–Fulcher (VTF) equation using Kaleida Graph software until all parameters converged to certain values.

The electrochemical windows of $[C_2C_1im][FSA]$ and M[FSA]–$[C_2C_1im][FSA]$ (x(M[FSA]) = 0.20) were determined by cyclic voltammetry at room temperature (~298 K) using an electrochemical apparatus (HZ-7000, Hokuto Denko Corp.). All the measurements were conducted using a three-electrode cell composed of a copper or glassy carbon disk working electrode, a platinum mesh counter electrode, and a silver wire reference electrode. Copper and glassy carbon working electrodes were used in the negative and positive potential regions, respectively. The reference electrode was separated from the main cell by a porous glass filter, which contained 50 mmol dm^{-3} silver trifluoromethanesulfonate ($AgCF_3SO_3$) in $[C_2C_1im][FSA]$ as the reference electrode electrolyte. Cyclic voltammetry measurements were started from rest potentials. The cut-off potentials (vs. Ag^+/Ag) in negative potential regions were set at −3.93 V (K), −3.48 V (Na), and −3.56 V (Li); those in positive potential regions were set at 1.70 V (K), 1.80 V (Na), and 1.80 V (Li). The scan rate was fixed at 5 mV s^{-1}.

3. RESULTS AND DISCUSSION

3.1 Physicochemical properties

Fig. 1 shows the phase diagram of the K[FSA]–$[C_2C_1im][FSA]$ system determined from DSC measurements. The DSC curves are collected in the Supplementary Information (Figs. S1–S11), and the DSC transition temperatures are summarized in Table S1. According to the phase diagram, compositions in the range of $0 \leq x$(K[FSA]) ≤ 0.20 are liquid well below 273 K. For example, the

end temperature of melting, T_{m_e}, at x(K[FSA]) = 0.20 is 256 K, which is almost the same as that of K[FSA]–[C_3C_1pyrr][FSA][9] and M[FSA]–[C_2C_1im][FSA] (M = Na[16], Li[15]) (see Table 5). As mentioned in the experimental section, the precipitation occurs in the melts of 0.30 ≤ x(K[FSA]) ≤ 0.90 after cooling to 298 K. Thus, in the phase diagram (Fig. 1), the liquidus line lies above 298 K at least in the compositional region higher than x(K[FSA]) = 0.30. According to the results of DSC measurements presented in Figs. S4–S10, the ionic liquids with the compositions of 0.30 ≤ x(K[FSA]) ≤ 0.90 possess the end of melting temperature higher than 360 K. As a consequence, a steep increase in T_{m_e} occurs near x(K[FSA]) = 0.30, which is also observed for K[FSA]–[C_3C_1pyrr][FSA].[9] The T_{m_e} value gradually increases at x(K[FSA]) > 0.30. Thus, the other physicochemical properties were measured at x(K[FSA]) = 0, 0.10 and 0.20. We further confirmed that a homogeneous liquid phase is maintained for more than one year at x(K[FSA]) = 0.25. Thus, the eutectic K[FSA]–[C_2C_1im][FSA] composition is considered to lie between x(K[FSA]) = 0.25 and 0.30. Further study is needed to determine the exact eutectic composition. According to the study on Li[FSA]–[C_2C_1im][FSA] system,[15] one crystallinity gap and one eutectic point were observed in Li[FSA]-poor region and at a Li[FSA]-rich composition, respectively. In addition, one line compound was confirmed at the composition of x(Li[FSA]) = 0.50. On the other hand, K[FSA]–[C_2C_1im][FSA] system has only one eutectic point at a K[FSA]-poor composition, and no line compounds exist. For reference, no line compounds were also reported for Na[FSA]–[C_2C_1im][FSA] system.[16] As a similar trend to the FSA-based ILs, the line compounds were reported for TFSA-based ILs containing Li salts.[18,19]

Fig. 2 shows Arrhenius plots of viscosity for K[FSA]–[C_2C_1im][FSA] ILs. Table 2 provides detailed η values at 273–388 K. The viscosity at x(K[FSA]) = 0.20 is 39.1 mPa s at 298 K, which is half that of the corresponding K[FSA]–[C_3C_1pyrr][FSA] system (78.2 mPa s at x(K[FSA]) =

0.20 and 298 K[9]). Table 5 summarizes the physicochemical properties of selected ILs containing imidazolium or pyrrolidinium cations. The viscosity of K[FSA]–[C_2C_1im][FSA] is less than that of its Na-based counterpart and slightly higher than that of its Li-based counterpart. The Arrhenius plots cannot be fitted by a straight line at any composition, which is a typical behavior of glass-like compounds.[20] The following VTF equation is applied to these compounds:

$$\eta(T) = A_\eta T^{1/2} \exp\left(\frac{B_\eta}{T - T_{0\eta}}\right) \quad (1)$$

where $T_{0\eta}$ is the ideal glass transition temperature, and A_η and B_η are constants related to the frequency factor and activation energy, respectively. The Arrhenius plots for all the K[FSA]–[C_2C_1im][FSA] ILs were fitted by the VTF equation. The fitting parameters are provided in Table S3.

Fig. 3 presents Arrhenius plots of ionic conductivity for the K[FSA]–[C_2C_1im][FSA] ILs. Table 3 summarizes detailed σ values at 258–388 K. The IL of x(K[FSA]) = 0.20 exhibits an ionic conductivity of 10.1 mS cm^{-1} at 298 K, which is twice as high as that of its counterpart of K[FSA]–[C_3C_1pyrr][FSA] system (4.8 mS cm^{-1} for x(K[FSA]) = 0.20 at 298 K).[9] Such differences in ionic conductivities are originated from the structure of these organic cations. According to the previous study,[21] the imidazolium cation have more planar structure than the pyrrolidinium cation, leading to the higher conductivity of the imidazolium-based ILs. The Arrhenius plots for each composition are fitted by the following VTF equation:

$$\sigma(T) = \frac{A_\sigma}{T^{1/2}} \exp\left(-\frac{B_\sigma}{T - T_{0\sigma}}\right) \quad (2)$$

where $T_{0\sigma}$ is the ideal glass transition temperature, and A_σ and B_σ are constants related to the frequency factor and activation energy, respectively. The fitting parameters are summarized in Table S3. Moreover, the ionic conductivity of K[FSA]–[C_2C_1im][FSA] is comparable to that of

typical organic solvent-based electrolytes. For example, the σ values are reported to be 10.7 mS cm^{-1} for 1 mol dm^{-3} K[FSA]/EC–DEC[5] and 10.85 mS cm^{-1} for 1 mol dm^{-3} KPF_6/EC–DMC[22] at 298 K, where EC = ethylene carbonate, DEC = diethyl carbonate, and DMC = dimethyl carbonate. It should be noted that the ionic conductivities are measured as the sum of conductivities of all the ionic species in the electrolytes. Thus, conductivities of K^+ ion (σ_{K^+}) are important to precisely evaluate the electrolyte properties for KIBs. However, few organized data of σ_{K^+} values have been provided in the preceding studies. Thus, in this study, the measured ionic conductivities are compared as a first step.

Fig. 4 shows density plots versus temperature for the K[FSA]–[C_2C_1im][FSA] ILs. Table 4 lists detailed ρ values from 273 to 368 K. First of all, the obtained density values of [C_2C_1im][FSA] IL are consistent with those in previous studies.[15,16,23,24] The density of all the compositions decreases linearly with temperature. Larger ρ values are obtained for compositions of higher K[FSA] content. According to Table 5, the density of M[FSA]–[C_2C_1im][FSA] (M = K, Na, Li) systems increases with increasing size of the alkali metal cation. The density of K[FSA]–[C_2C_1im][FSA] is approximately 7% higher than that of K[FSA]–[C_3C_1pyrr][FSA]. Such higher ρ values of imidazolium-based ILs versus pyrrolidinium-based ones have been reported for ionic liquids containing the $TFSA^-$ anion.[25,26] The molar concentrations of K^+ cations in K[FSA]–[C_2C_1im][FSA] electrolytes with x(K[FSA]) = 0.10 and 0.20 are calculated from their densities and linearly fitted to temperature, as listed in Table S2. Table 5 reveals that the molar concentrations of alkali metal cations ($C(M^+)$; M = K, Na, Li) in all the M[FSA]–[C_2C_1im][FSA] ILs are approximately 1.1 mol dm^{-3} at x(M[FSA]) = 0.20. Thus, no clear difference is observed among the alkali metal cations in the ILs. These $C(M^+)$ values are approximately 10% higher than those of M[FSA]–[C_3C_1pyrr][FSA] ILs at x(M[FSA]) = 0.20,[9,27,28] which reflects the denser nature

of the $C_2C_1im^+$ cation.

Table 6 summarizes the end temperatures of melting (T_{m_e}) and other physicochemical properties of K[X]–[Ocat][X] (X = FSA, TFSA; Ocat = C_2C_1im, C_3C_1pyrr) electrolytes. The T_{m_e} values of these ILs lie at around 260 K except for K[TFSA]–[C_3C_1pyrr][TFSA], for which the T_{m_e} value is reported to be 280–290 K.[29] The FSA-based ILs show smaller viscosities and higher conductivities than the TFSA-based ILs. The same trend has been already reported in the case of IL electrolytes for LIBs[12,15,30] and NIBs[16,31]. For example, K[FSA]–[C_2C_1im][FSA] at x(K[FSA]) = 0.10, which corresponds to $C(K^+)$ = 0.521 mol dm^{-3}, exhibits more than twice the conductivity of K[TFSA]–[C_2C_1im][TFSA] at $C(K^+)$ = 0.5 mol dm^{-3}.

Fig. 5 shows the Walden plots of the K[FSA]–[C_2C_1im][FSA] ILs. All the plots lie slightly lower and to the right of the ideal KCl line. The linear log–log behavior of these ILs is expressed in terms of the fractional Walden rule:[32–34]

$$\lambda\eta^{\alpha} = \text{const.} \quad (3)$$

where λ is the molar conductivity (S cm^2 mol^{-1}), and α is a constant ($0 < \alpha < 1$) corresponding to the slope of the Walden plot. Table S4 provides the slope, α, and vertical intercept, C' = log($\lambda\eta^{\alpha}$), values of K[FSA]–[Ocat][FSA] (Ocat = C_2C_1im, C_3C_1pyrr) ILs. The imidazolium- and pyrrolidinium-based ILs exhibit similar α and C' values. Thus, no special trends are observed for these ILs.

3.2 Electrochemical properties

Cyclic voltammetry measurements were conducted to evaluate the electrochemical stability of the M[FSA]–[C_2C_1im][FSA] electrolytes. We first investigated the electrochemical stability of pure [C_2C_1im][FSA], as shown in Fig. S12. During the cathodic potential sweep in the negative

potential region, the reductive current begins to flow from ca. −2.0 V vs. Ag^+/Ag and sharply increases at −2.8 V, which is consistent with previous reports and is considered to arise from decomposition of the $C_2C_1im^+$ cation.[12,35] In the positive potential region, the steep increase in oxidative current is observed from ca. 1.5 V, which is attributed to decomposition of the FSA^- anion.[12] The cathodic (E_{CL}) and anodic (E_{AL}) limit potentials are defined as the values where the current densities reach −0.1 and +0.1 mA cm^{-2} during the cathodic and anodic potential sweeps, respectively. The values are $E_{CL} = -2.52$ and $E_{AL} = +1.51$ V vs. Ag^+/Ag. Thus, the electrochemical window (EW) is 4.03 V.

Fig. S13 compares initial cyclic voltammograms of copper disks in M[FSA]–$[C_2C_1im][FSA]$ (x(M[FSA]) = 0.20; M = K, Na, Li). Small irreversible reductive current peaks are observed at around −3.0 V for all the systems. Judging from the results for pure $[C_2C_1im][FSA]$, these currents correspond to the decomposition of the $C_2C_1im^+$ cation. The addition of an alkali metal salt to $[C_2C_1im][FSA]$ suppresses the decomposition of the electrolyte. Such extension of the cathodic limit has been reported in FSA-based IL electrolytes containing Li^+[35] and Na^+[36] cations and is explained by the formation of a solid electrolyte interphase (SEI) on the electrode surface. A similar phenomenon is believed to occur in K[FSA]–$[C_2C_1im][FSA]$. The redox potential of the alkali metals, $E(M^+/M)$, is defined as the potential at which the current density reaches zero after reversing the sweep direction from negative to positive. We regard the $E(M^+/M)$ values as E_{CL} for the M[FSA]–$[C_2C_1im][FSA]$ systems.

Fig. 6 compares cyclic voltammograms obtained in M[FSA]–$[C_2C_1im][FSA]$ (x(M[FSA]) = 0.20; M = K, Na, Li) ILs. It should be noted that voltammograms in the negative potential region were measured at a copper electrode in the 2nd cycle. As with the 1st cycles in Fig. S13, the cathodic stability is limited by alkali metal deposition, *i.e.* $E_{CL} = E(M^+/M)$. A small cathodic peak

is observed at around −3 V in the 1st cycle in all the ILs, but is barely apparent in the 2nd cycle. This indicates that successive electrolyte decomposition is suppressed by SEI formation in the 1st cycle. The E_{AL} values of all the ILs are almost identical to those of pure $[C_2C_1im][FSA]$. Thus, the anodic stability is determined by the decomposition of the FSA^- anion.

Table 7 summarizes the limit potentials and electrochemical windows of the ILs. The $E(M^+/M)$ values of the M[FSA]–$[C_2C_1im][FSA]$ ILs are −3.69 (K), −3.34 (Na), and −3.44 (Li) V vs. Ag^+/Ag. In our previous report on M[FSA]–$[C_3C_1pyrr][FSA]$ ILs,[9] the $E(M^+/M)$ values were −3.71 (K), −3.35 (Na), and −3.46 (Li) V vs. Ag^+/Ag. Thus, the effect of the organic cation on the cathodic limit potential is negligible in the FSA-based ILs. The $E(K^+/K)$ value is most negative for both the imidazolium- and pyrrolidinium-based ILs, which produces the widest electrochemical window in K-based ILs among the alkali metal-ion systems. The EW values of M[FSA]–$[C_2C_1im][FSA]$ ILs are 5.19 (K), 4.91 (Na), and 4.95 (Li) V, which indicates the advantages of K[FSA]–$[C_2C_1im][FSA]$ IL electrolyte for novel KIBs having higher operating voltages than LIBs.

4. CONCLUSIONS

We have evaluated the properties of K[FSA]–$[C_2C_1im][FSA]$ ionic liquids as electrolytes for KIBs. The phase diagram determined by DSC indicates that binary mixtures exist as a liquid below 273 K at molar fractions of $x(K[FSA]) \leq 0.20$. Physicochemical properties were investigated for selected liquid compositions. For example, ionic conductivity equals 10.1 mS cm^{-1} at 298 K at $x(K[FSA]) = 0.20$, which corresponds to a K^+ ion concentration of ca. 1 mol dm^{-3}. This value is higher than that of other IL electrolytes for KIBs and is comparable to those of organic solvent-based electrolytes for KIBs. Cyclic voltammetry measurements were conducted to determine the electrochemical stability of M[FSA]–$[C_2C_1im][FSA]$ ($x(M[FSA]) = 0.20$; M = K, Na, Li) ILs. The

electrochemical window of the K-based IL is 5.19 V, which is wider than that of the Na- and Li-based ILs due to the more negative K^+/K potential. Therefore, the conductive K[FSA]–[C_2C_1im][FSA] electrolyte system is a potential candidate for use in high-voltage KIBs.

■ ASSOCIATED CONTENT

Supporting Information Available:

Physicochemical properties, VTF parameters, Walden plot parameters, DSC curves, and cyclic voltammograms (PDF)

■ AUTHOR INFORMATION

Corresponding Author

*E-mail: yamamoto.takayuki.2w@kyoto-u.ac.jp, Tel: +81-774-38-3498, Fax: +81-774-38-3499 (T.Y.)

Notes

The authors declare no competing financial interest.

■ ACKNOWLEDGMENTS

This study was partly supported by JSPS KAKENHI grant (JP18K14320) and the research grant from the Kansai Research Foundation for Technology Promotion. We appreciate Nippon Shokubai Co., Ltd. for supplying K[FSA] and Na[FSA] salts.

■ REFERENCES

(1) Watanabe, M.; Thomas, M. L.; Zhang, S.; Ueno, K.; Yasuda, T.; Dokko, K. Application of Ionic Liquids to Energy Storage and Conversion Materials and Devices. *Chem. Rev.* **2017**, *117*, 7190–7239.

(2) Hagiwara, R.; Matsumoto, K.; Hwang, J.; Nohira, T. Sodium Ion Batteries using Ionic Liquids as Electrolytes. *Chem. Rec.* **2018**, *18*, 1–14.

(3) Matsumoto, K.; Hwang, J.; Kaushik, S.; Chen, C.-Y.; Hagiwara, R. Advances in sodium secondary batteries utilizing ionic liquid electrolytes. *Energy Environ. Sci.* **2019**, *12*, 3247–3287.

(4) Yamamoto, T.; Nishijima, S.; Nohira, T. Comparative Study of M[N(SO_2F)(SO_2CF_3)]–[*N*-Butyl-*N*-methylpyrroridinium][N(SO_2F)(SO_2CF_3)] (M = Li, Na, K, Rb, Cs) Ionic Liquid Electrolytes. *J. Phys. Chem. B* **2020**, *124*, 8380–8387.

(5) Komaba, S.; Hasegawa, T.; Dahbi, M.; Kubota, K. Potassium intercalation into graphite to realize high-voltage/high-power potassium-ion batteries and potassium-ion capacitors, *Electrochem. Commun.* **2015**, *60*, 172–175.

(6) Kubota, K.; Dahbi, M.; Hosaka, T.; Kumakura, S.; Komaba, S. Towards K-Ion and Na-Ion Batteries as “Beyond Li-Ion”. *Chem. Rec.* **2018**, *18*, 1–22.

(7) Marcus, Y. Thermodynamic Functions of Transfer of Single Ions from Water to Nonaqueous and Mixed Solvents, PART 3: Standard Potentials of Selected Electrodes. *Pure Appl. Chem.* **1985**, *57*, 1129–1132.

(8) Watarai, A.; Kubota, K.; Yamagata, M.; Goto, T.; Nohira, T.; Hagiwara, R.; Ui, K.; Kumagai, N. A rechargeable lithium metal battery operating at intermediate temperatures using molten alkali bis(trifluoromethylsulfonyl)amide mixture as an electrolyte. *J. Power Sources* **2008**,

183, 724–729.

(9) Yamamoto, T.; Matsumoto, K.; Hagiwara, R.; Nohira, T. Physicochemical and Electrochemical Properties of K[$N(SO_2F)_2$]–[*N*-Methyl-*N*-propylpyrrolidinium][$N(SO_2F)_2$] Ionic Liquids for Potassium-Ion Batteries. *J. Phys. Chem. C* **2017**, *121*, 18450–18458.

(10) Yamamoto, T.; Nohira, T. Tin negative electrodes using an FSA-based ionic liquid electrolyte: improved performance of potassium secondary batteries. *Chem. Comm.* **2020**, *56*, 2538–2541.

(11) Onuma, H.; Kubota, K.; Muratsubaki, S.; Hosaka, T.; Tatara, R.; Yamamoto, T.; Matsumoto, K.; Nohira, T.; Hagiwara, R.; Oji, H. Application of Ionic Liquid as K-Ion Electrolyte of Graphite//$K_2Mn[Fe(CN)_6]$ Cell. *ACS Energy Lett.* **2020**, 5, 2849–2857.

(12) Matsumoto, H.; Sakaebe, H.; Tatsumi, K.; Kikuta, M.; Ishiko, E.; Kono, M. Fast cycling of Li/$LiCoO_2$ cell with low-viscosity ionic liquids based on bis(fluorosulfonyl)imide $[FSI]^-$. *J. Power Sources* **2006**, *160*, 1308–1313.

(13) Ishikawa, M.; Sugimoto, T.; Kikuta, M.; Ishiko, E.; Kono, M. Pure ionic liquid electrolytes compatible with a graphitized carbon negative electrode in rechargeable lithium-ion batteries. *J. Power Sources* **2006**, *162*, 658–662.

(14) Guerfi, A.; Duchesne, S.; Kobayashi, Y.; Vijh, A.; Zaghib, K. $LiFePO_4$ and graphite electrodes with ionic liquids based on bis(fluorosulfonyl)imide $(FSI)^-$ for Li-ion batteries. *J. Power Sources* **2008**, *175*, 866–873.

(15) Matsumoto, K.; Nishiwaki, E.; Hosokawa, T.; Tawa, S.; Nohira, T.; Hagiwara, R. Thermal, Physical, and Electrochemical Properties of Li[$N(SO_2F)_2$]-[1-Ethyl-3-methylimidazolium][$N(SO_2F)_2$] Ionic Liquid Electrolytes for Li Secondary Batteries Operated at Room and Intermediate Temperatures. *J. Phys. Chem. C* **2017**, *121*, 9209–9219.

(16) Matsumoto, K.; Hosokawa, T.; Nohira, T.; Hagiwara, R.; Fukunaga, A.; Numata, K.; Itani, E.; Sakai, S.; Nitta, K.; Inazawa, S. The Na[FSA]–[C_2C_1im][FSA] ($C_2C_1im^+$:1-ethyl-3-methylimidazolium and FSA^-:bis(fluorosulfonyl)amide) ionic liquid electrolytes for sodium secondary batteries. *J. Power Sources* **2014**, *265*, 36–39.

(17) Chen, C.-Y.; Kiko, T.; Hosokawa, T.; Matsumoto, K.; Nohira, T.; Hagiwara, R. Ionic liquid electrolytes with high sodium ion fraction for high-rate and long-life sodium secondary batteries. *J. Power Sources* **2016**, *332*, 51–59.

(18) Henderson, W. A.; Passerini, S. Phase Behavior of Ionic Liquid–LiX Mixtures: Pyrrolidinium Cations and $TFSI^-$ Anions. *Chem. Mater.* **2004**, *16*, 2881–2885.

(19) Zhou, Q.; Boyle, P. D.; Malpezzi, L.; Mele, A.; Shin, J.-H.; Passerini, S.; Henderson, W. A. Phase Behavior of Ionic Liquid–LiX Mixtures: Pyrrolidinium Cations and $TFSI^-$ Anions − Linking Structure to Transport Properties. *Chem. Mater.* **2011**, *23*, 4331–4337.

(20) Easteal, A. J.; Angell, C. A. Viscosity of Molten $ZnCl_2$ and Supercritical Behavior in Its Binary Solutions. *J. Chem. Phys.* **1972**, *56*, 4231–4233.

(21) McFarlane, D. R.; Sun, J.; Golding, J.; Meakin, P.; Forsyth, M. High conductivity molten salts based on the imide ion. *Electrochim. Acta* **2000**, *45*, 1271–1278.

(22) Amara, S.; Toulc'Hoat, J.; Timperman, L.; Biller, A.; Galiano, H.; Marcel, C.; Ledigabel M.; Anouti, M. Comparative Study of Alkali-Cation-Based (Li^+, Na^+, K^+) Electrolytes in Acetonitrile and Alkylcarbonates. *ChemPhysChem* **2019**, *20*, 581–594.

(23) Seki, S.; Tsuzuki, S.; Hayamizu, K.; Umebayashi, Y.; Serizawa, N.; Takei, K.; Miyashiro, H. Comprehensive Refractive Index Property for Room-Temperature Ionic Liquids. *J. Chem. Eng. Data* **2012**, *57*, 2211–2216.

(24) Sas, O. G.; Ivanis, G. R.; Kijevcanin, M. L.; Gonzalez, B.; Dominguez, A.; Radovic, I. R. Densities and Derived Volumetric Properties of Ionic Liquids with [Nf2] and [NTf2] Anions at High Pressures. *J. Chem. Eng. Data* **2018**, *63*, 954–964.

(25) Tokuda, H.; Ishii, K.; Abu Bin Hasan Susan, Md.; Tsuzuki, S.; Hayamizu, K.; Watanabe, M. Physicochemical Properties and Structures of Room-Temperature Ionic Liquids. 3. Variation of Cationic Structures. *J. Phys. Chem. B* **2006**, *110*, 2833–2839.

(26) Tokuda, H.; Hayamizu, K.; Ishii, K.; Abu Bin Hasan Susan, Md.; Watanabe, M. Physicochemical Properties and Structures of Room Temperature Ionic Liquids. 2. Variation of Alkyl Chain Length in Imidazolium Cation. *J. Phys. Chem. B* **2005**, *109*, 6103–6110.

(27) Yoon, H.; Best, A. S.; Forsyth, M.; MacFarlane, D. R.; Howlett, P. C. Physical properties of high Li-ion content *N*-propyl-*N*-methylpyrrolidinium bis(fluorosulfonyl)imide based ionic liquid electrolytes. *Phys. Chem. Chem. Phys.* **2015**, *17*, 4656–4663.

(28) Matsumoto, K.; Okamoto, Y.; Nohira, T.; Hagiwara, R. Thermal and Transport Properties of Na[$N(SO_2F)_2$]–[*N*-Methyl-*N*-propylpyrrolidinium][$N(SO_2F)_2$] Ionic Liquids for Na Secondary Batteries. *J. Phys. Chem. C* **2015**, *119*, 7648−7655.

(29) Yoshii, K.; Masese, T.; Kato, M.; Kubota, K.; Senoh, H.; Shikano, M. Sulfonylamide-Based Ionic Liquids for High-Voltage Potassium-Ion Batteries with Honeycomb Layered Cathode Oxides. *ChemElectroChem* **2019**, *6*, 3901–3910.

(30) Seki, S.; Kobayashi, Y.; Miyashiro, H.; Ohno, Y.; Usami, A.; Mita, Y.; Kihira, N.; Watanabe, M.; Terada, N. Lithium Secondary Batteries Using Modified-Imidazolium Room-Temperature Ionic Liquid. *J. Phys. Chem. B* **2006**, *110*, 10228–10230.

(31) Monti, D.; Jónsson, E.; Palacín, M. R.; Johansson, P. Ionic liquid based electrolytes for sodium-ion batteries: Na^+ solvation and ionic conductivity. *J. Power Sources* **2014**, *245*, 630–636.

(32) Pugsley, F. A.; Westmore, F. E. W. Molten Salts: Viscosity of Silver Nitrate. *Can. J. Chem.* **1954**, *32*, 839–841.

(33) Xu, W.; Angell, C. A. Solvent-Free Electrolytes with Aqueous Solution-Like Conductivities. *Science* **2003**, *302*, 422–425.

(34) Xu, W.; Cooper, E. I.; Angell, C. A. Ionic Liquids: Ion Mobilities, Glass Temperatures, and Fragilities. *J. Phys. Chem. B* **2003**, *107*, 6170–6178.

(35) Yamagata, M.; Nishigaki, N.; Nishishita, S.; Matsui, Y.; Sugimoto, T.; Kikuta, M.; Higashizaki, T.; Kono, M.; Ishikawa, M. Charge–discharge behavior of graphite negative electrodes in bis(fluorosulfonyl)imide-based ionic liquid and structural aspects of their electrode/electrolyte interfaces. *Electrochim. Acta* **2013**, *110*, 181–190.

(36) Hosokawa, T.; Matsumoto, K.; Nohira, T.; Hagiwara, R.; Fukunaga, A.; Sakai, S.; Nitta, K.; Stability of Ionic Liquids against Sodium Metal: A Comparative Study of 1-Ethyl-3-methylimidazolium Ionic Liquids with Bis(fluorosulfonyl)amide and Bis(trifluoromethylsulfonyl)amide. *J. Phys. Chem. C* **2016**, *120*, 9628–9636.

■ TABLES AND FIGURES

Table 1 Summary of chemical reagents used in this study.

chemical	CAS Reg. No.	supplier	purity / mass%	purification method	water content / ppm
$[C_2C_1im][FSA]$	235789-75-0	Kanto Chemical Co., Inc.	≥ 99	vacuum drying	< 50
Li[FSA]	171611-11-3	Kishida Chemical Co., Ltd.	99	vacuum drying	< 50
Na[FSA]	100669-96-3	Nippon Shokubai Co., Ltd.	≥ 99	vacuum drying	< 50
K[FSA]	14984-76-0	Nippon Shokubai Co., Ltd.	99	vacuum drying	< 50
$Ag[CF_3SO_3]$	2923-28-6	Sigma-Aldrich, Inc.	≥ 99	–	–

Table 2 Viscosities (η; mPa s) of the K[FSA]–[C_2C_1im][FSA] (x(K[FSA]) = 0, 0.10, 0.20) ionic liquids at 101.3 kPa.[a]

T [b] / K	η [c] / mPa s		
	x(K[FSA]) [d]		
	0	0.10	0.20
273	$45._9 \pm 1._4$	$71._0 \pm 2._1$	$119 \pm 3._6$
278	$37._5 \pm 1._1$	$56._3 \pm 1._7$	$91._4 \pm 2._7$
283	$31._2 \pm 0.9$	$45._7 \pm 1._4$	$71._7 \pm 2._2$
288	$26._2 \pm 0.8$	$37._5 \pm 1._1$	$57._4 \pm 1._7$
293	$22._3 \pm 0.7$	$31._4 \pm 0.9$	$46._6 \pm 1._4$
298	$19._2 \pm 0.6$	$26._6 \pm 0.8$	$39._1 \pm 1._2$
303	$16._7 \pm 0.5$	$22._7 \pm 0.7$	$32._8 \pm 1._0$
308	$14._6 \pm 0.4$	$19._6 \pm 0.6$	$27._7 \pm 0.8$
313	$12._9 \pm 0.4$	$17._0 \pm 0.5$	$23._8 \pm 0.7$
318	$11._4 \pm 0.3$	$14._9 \pm 0.4$	$20._6 \pm 0.6$
323	$10._2 \pm 0.3$	$13._1 \pm 0.4$	$18._1 \pm 0.5$
328	$9.1_1 \pm 0.2_7$	$11._6 \pm 0.3$	$15._7 \pm 0.5$
333	$8.2_2 \pm 0.2_5$	$10._4 \pm 0.3$	$13._8 \pm 0.4$
338	$7.4_5 \pm 0.2_2$	$9.3_0 \pm 0.2_8$	$12._2 \pm 0.4$
343	$6.7_9 \pm 0.2_0$	$8.3_8 \pm 0.2_5$	$10._8 \pm 0.3$
348	$6.2_2 \pm 0.1_9$	$7.6_1 \pm 0.2_3$	$9.8_1 \pm 0.2_9$
353	$5.7_4 \pm 0.1_7$	$6.9_5 \pm 0.2_1$	$8.8_4 \pm 0.2_7$
358	$5.3_2 \pm 0.1_6$	$6.3_9 \pm 0.1_9$	$7.9_8 \pm 0.2_4$
363	$4.9_6 \pm 0.1_5$	$5.9_1 \pm 0.1_8$	$7.3_1 \pm 0.2_2$
368	$4.6_5 \pm 0.1_4$	$5.5_0 \pm 0.1_7$	$6.7_5 \pm 0.2_0$
373	$4.4_0 \pm 0.1_3$	$5.1_6 \pm 0.1_5$	$6.2_6 \pm 0.1_9$
378	$4.1_3 \pm 0.1_2$	$4.8_0 \pm 0.1_4$	$5.7_8 \pm 0.1_7$
383	$3.8_8 \pm 0.1_2$	$4.4_9 \pm 0.1_3$	$5.3_6 \pm 0.1_6$
388	$3.6_6 \pm 0.1_1$	$4.2_0 \pm 0.1_3$	$4.9_8 \pm 0.1_5$

Expanded uncertainties (U) are as follows: [a] $U(p)$ = 10 kPa, (0.95 level of confidence); p: pressure. [b] $U(T)$ = 0.1 K, (0.95 level of confidence). [c] $\eta \pm U(\eta)$, (0.95 level of confidence). [d] $U(x(\text{K[FSA]}))$ = 0.002 (x(K[FSA]) = 0.10 and 0.20), (0.95 level of confidence).

Table 3 Ionic conductivities (σ; mS cm^{-1}) of the K[FSA]–[C_2C_1im][FSA] (x(K[FSA]) = 0, 0.10, 0.20) ionic liquids at 101.3 kPa.[a]

T [b] / K	σ [c] / mS cm^{-1}		
	x(K[FSA]) [d]		
	0	0.10	0.20
258	–	–	$1.4_9 \pm 0.07$
263	–	$3.3_2 \pm 0.1_7$	$2.0_6 \pm 0.1_0$
268	$5.9_5 \pm 0.3_0$	$4.2_7 \pm 0.2_1$	$2.7_7 \pm 0.1_4$
273	$7.3_0 \pm 0.3_6$	$5.3_9 \pm 0.2_7$	$3.6_1 \pm 0.1_8$
278	$8.8_0 \pm 0.4_4$	$6.6_6 \pm 0.3_3$	$4.6_1 \pm 0.2_3$
283	$10._5 \pm 0.5$	$8.0_8 \pm 0.4_0$	$5.7_5 \pm 0.2_9$
288	$12._3 \pm 0.6$	$9.6_6 \pm 0.4_8$	$7.0_6 \pm 0.3_5$
293	$14._3 \pm 0.7$	$11._4 \pm 0.6$	$8.5_0 \pm 0.4_2$
298	$16._4 \pm 0.8$	$13._3 \pm 0.7$	$10._1 \pm 0.5$
303	$18._6 \pm 0.9$	$15._3 \pm 0.8$	$11._9 \pm 0.6$
308	$21._0 \pm 1._0$	$17._5 \pm 0.9$	$13._8 \pm 0.7$
313	$23._5 \pm 1._2$	$19._8 \pm 1._0$	$15._9 \pm 0.8$
318	$26._1 \pm 1._3$	$22._2 \pm 1._1$	$18._1 \pm 0.9$
323	$28._9 \pm 1._4$	$24._8 \pm 1._2$	$20._4 \pm 1._0$
328	$31._8 \pm 1._6$	$27._5 \pm 1._4$	$22._9 \pm 1._1$
333	$34._8 \pm 1._7$	$30._4 \pm 1._5$	$25._4 \pm 1._3$
338	$37._9 \pm 1._9$	$33._3 \pm 1._7$	$28._3 \pm 1._4$
343	$41._3 \pm 2._1$	$36._2 \pm 1._8$	$31._2 \pm 1._6$
348	$44._7 \pm 2._2$	$39._4 \pm 2._0$	$34._2 \pm 1._7$
353	$48._2 \pm 2._4$	$42._7 \pm 2._1$	$37._4 \pm 1._9$
358	$51._9 \pm 2._6$	$46._1 \pm 2._3$	$40._6 \pm 2._0$
363	$55._7 \pm 2._8$	$49._7 \pm 2._5$	$44._0 \pm 2._2$
368	$59._7 \pm 3._0$	$53._4 \pm 2._7$	$47._4 \pm 2._4$
373	$63._6 \pm 3._2$	$57._2 \pm 2._9$	$51._0 \pm 2._5$
378	$68._1 \pm 3._4$	$61._3 \pm 3._1$	$54._5 \pm 2._7$
383	$73._1 \pm 3._7$	$65._2 \pm 3._3$	$58._1 \pm 2._9$
388	$78._6 \pm 3._9$	$69._4 \pm 3._5$	$61._8 \pm 3._1$

Expanded uncertainties (U) are as follows: [a] $U(p)$ = 10 kPa, (0.95 level of confidence); p: pressure. [b] $U(T)$ = 0.1 K, (0.95 level of confidence). [c] $\sigma \pm U(\sigma)$, (0.95 level of confidence). [d] $U(x(\text{K[FSA]}))$ = 0.002 (x(K[FSA]) = 0.10 and 0.20), (0.95 level of confidence).

Table 4 Densities (ρ; g cm^{-3}) and their fitting parameters of the K[FSA]–[C_2C_1im][FSA] (x(K[FSA]) = 0, 0.10, 0.20) ionic liquids at 101.3 kPa.[a]

T [b] / K	ρ [c] / g cm^{-3}		
	x(K[FSA]) [d]		
	0	0.10	0.20
273	$1.46_5 \pm 0.001$	$1.50_4 \pm 0.002$	$1.54_7 \pm 0.002$
278	$1.46_0 \pm 0.001$	$1.49_9 \pm 0.001$	$1.54_2 \pm 0.002$
283	$1.45_6 \pm 0.001$	$1.49_5 \pm 0.001$	$1.53_7 \pm 0.002$
288	$1.45_1 \pm 0.001$	$1.49_0 \pm 0.001$	$1.53_2 \pm 0.002$
293	$1.44_6 \pm 0.001$	$1.48_5 \pm 0.001$	$1.52_8 \pm 0.002$
298	$1.44_2 \pm 0.001$	$1.48_0 \pm 0.001$	$1.52_3 \pm 0.002$
303	$1.43_7 \pm 0.001$	$1.47_6 \pm 0.001$	$1.51_8 \pm 0.002$
308	$1.43_3 \pm 0.001$	$1.47_1 \pm 0.001$	$1.51_3 \pm 0.002$
313	$1.42_8 \pm 0.001$	$1.46_6 \pm 0.001$	$1.50_8 \pm 0.002$
318	$1.42_4 \pm 0.001$	$1.46_2 \pm 0.001$	$1.50_4 \pm 0.002$
323	$1.41_9 \pm 0.001$	$1.45_7 \pm 0.001$	$1.49_9 \pm 0.001$
328	$1.41_5 \pm 0.001$	$1.45_3 \pm 0.001$	$1.49_4 \pm 0.001$
333	$1.41_0 \pm 0.001$	$1.44_8 \pm 0.001$	$1.49_0 \pm 0.001$
338	$1.40_6 \pm 0.001$	$1.44_4 \pm 0.001$	$1.48_5 \pm 0.001$
343	$1.40_1 \pm 0.001$	$1.43_9 \pm 0.001$	$1.48_0 \pm 0.001$
348	$1.39_7 \pm 0.001$	$1.43_5 \pm 0.001$	$1.47_6 \pm 0.001$
353	$1.39_3 \pm 0.001$	$1.43_0 \pm 0.001$	$1.47_1 \pm 0.001$
358	$1.38_8 \pm 0.001$	$1.42_6 \pm 0.001$	$1.46_7 \pm 0.001$
363	$1.38_4 \pm 0.001$	$1.42_1 \pm 0.001$	$1.46_2 \pm 0.001$
368	$1.38_0 \pm 0.001$	$1.41_7 \pm 0.001$	$1.45_8 \pm 0.001$
$A_\rho \times 10^4$ *	-8.99_6	-9.17_4	-9.41_2
B_ρ *	1.71_0	1.75_4	1.80_4
R^2 **	0.9998_6	0.9998_6	0.9998_5

*Density values were fitted by the following equation: $\rho = A_\rho T + B_\rho$

**R^2: coefficient of determination

Expanded uncertainties (U) are as follows: [a]$U(p)$ = 10 kPa, (0.95 level of confidence); p: pressure. [b]$U(T)$ = 0.1 K, (0.95 level of confidence). [c]$\rho \pm U(\rho)$, (0.95 level of confidence). [d]$U(x\text{(K[FSA])}) = 0.002$ (x(K[FSA]) = 0.10 and 0.20), (0.95 level of confidence).

Table 5 Summary of end temperatures of melting (T_{m_e}) and other physicochemical properties (η: viscosity, σ: ionic conductivity, ρ: density, $C(M^+)$: molar concentration of alkali metal cation)at 298 K of M[FSA]–[C_2C_1im][FSA] (molar fraction of M[FSA]: x(M[FSA]) = 0.20; M = K, Na, Li) and K[FSA]–[C_3C_1pyrr][FSA] (x(K[FSA]) = 0.20) ILs.

IL	T_{m_e} / K	η / mPa s	σ / mS cm^{-1}	ρ / g cm^{-3}	$C(M^+)$ / mol dm^{-3}
K[FSA]–[C_2C_1im][FSA][a]	256[b]	39.1[c]	10.1[d]	1.523[e]	1.100[f]
Na[FSA]–[C_2C_1im][FSA][16]	251	43.4	8.5	1.519	1.110
Li[FSA]–[C_2C_1im][FSA][15]	254	36.3	10.1	1.501	1.110
K[FSA]–[C_3C_1pyrr][FSA][9]	256	78.2	4.8	1.429	0.977

Expanded uncertainties (U) are as follows: [a]$U(x(K[FSA])) = 0.002$, (0.95 level of confidence). [b]$U(T_{m\_e}) = 1$ K, (0.95 level of confidence). [c]$U(\eta) = 1.2$ mPa s, (0.95 level of confidence). [d]$U(\sigma) = 0.5$ mS cm^{-1}, (0.95 level of confidence). [e]$U(\rho) = 0.002$ g cm^{-3}, (0.95 level of confidence). [f]$U(C(K^+)) = 0.001$ mol dm^{-3}, (0.95 level of confidence).

Table 6 Summary of end temperatures of melting (T_{m_e}) and other physicochemical properties (x(K[X]): molar fraction of K[X], η: viscosity, σ: ionic conductivity, ρ: density, $C(K^+)$: molar concentration of K^+ ion) at 298 K for K[X]–[Ocat][X] ILs (X = FSA, TFSA; Ocat = C_2C_1im, C_3C_1pyrr).

IL	x(K[FSA]) or x(K[TFSA])	T_{m_e} / K	η / mPa s	σ / mS cm^{-1}	ρ / g cm^{-3}	$C(K^+)$ / mol dm^{-3}
K[FSA]–[C_2C_1im][FSA]	0	263[b]	19.2[c]	16.4[d]	1.442[e]	0
	0.10[a]	260[b]	26.6[c]	13.3[d]	1.480[e]	0.5210[f]
	0.20[a]	256[b]	39.1[c]	10.1[d]	1.523[e]	1.100[f]
K[FSA]–[C_3C_1pyrr][FSA][9]	0	269	40.6	8.4	1.339	0
	0.10	261	55.6	6.6	1.377	0.460
	0.20	256	78.2	4.8	1.420	0.977
K[TFSA]–[C_2C_1im][TFSA][29]	0	~260	32	9.2	1.519	0
	0.12*	~255	58	5.7	1.559	0.5
K[TFSA]–[C_3C_1pyrr][TFSA][29]	0	~290	60	3.9	1.428	0
	0.13*	~280	119	2.1	1.474	0.5

*Molar fractions of K[TFSA] were calculated using ρ and $C(K^+)$ values.

Expanded uncertainties (U) are as follows: [a]$U(x(\text{K[FSA]})) = 0.002$, (0.95 level of confidence). [b]$U(T_{m\_e}) =$ 1 K, (0.95 level of confidence). [c]$U(\eta) = 0.6$ mPa s (x(K[FSA]) = 0), 0.8 mPa s (x(K[FSA]) = 0.10), and 1.2 mPa s (x(K[FSA]) = 0.20), (0.95 level of confidence). [d]$U(\sigma) = 0.8$ mS cm^{-1} (x(K[FSA]) = 0), 0.7 mS cm^{-1} (x(K[FSA]) = 0.10), and 0.5 mS cm^{-1} (x(K[FSA]) = 0.20), (0.95 level of confidence). [e]$U(\rho) =$ 0.001 g cm^{-3} (x(K[FSA]) = 0 and 0.10) and 0.002 g cm^{-3} (x(K[FSA]) = 0.20), (0.95 level of confidence). [f]$U(C(K^+)) = 0.0005$ mol dm^{-3} (x(K[FSA]) = 0.10) and 0.001 mol dm^{-3} (x(K[FSA]) = 0.20), (0.95 level of confidence).

Table 7 Summary of cathodic (E_{CL}) and anodic (E_{AL}) limit potentials and electrochemical windows (EW) of M[FSA]–[C_2C_1im][FSA] (molar fraction of M[FSA]: x(M[FSA]) = 0.20; M = K, Na, Li) ionic liquids.

	Limit potential / V vs. Ag^+/Ag		EW / V
	E_{CL} [a]	E_{AL} [b]	
M = K	−3.69	1.50	5.19
M = Na	−3.34	1.57	4.91
M = Li	−3.44	1.51	4.95

[a] E_{CL} is defined as the zero-current potential of the cyclic voltammograms, $E_{CL} = E(M^+/M)$.
[b] E_{AL} is defined as the potential at which the current density reaches 0.1 mA cm^{-2} on the positive scan.

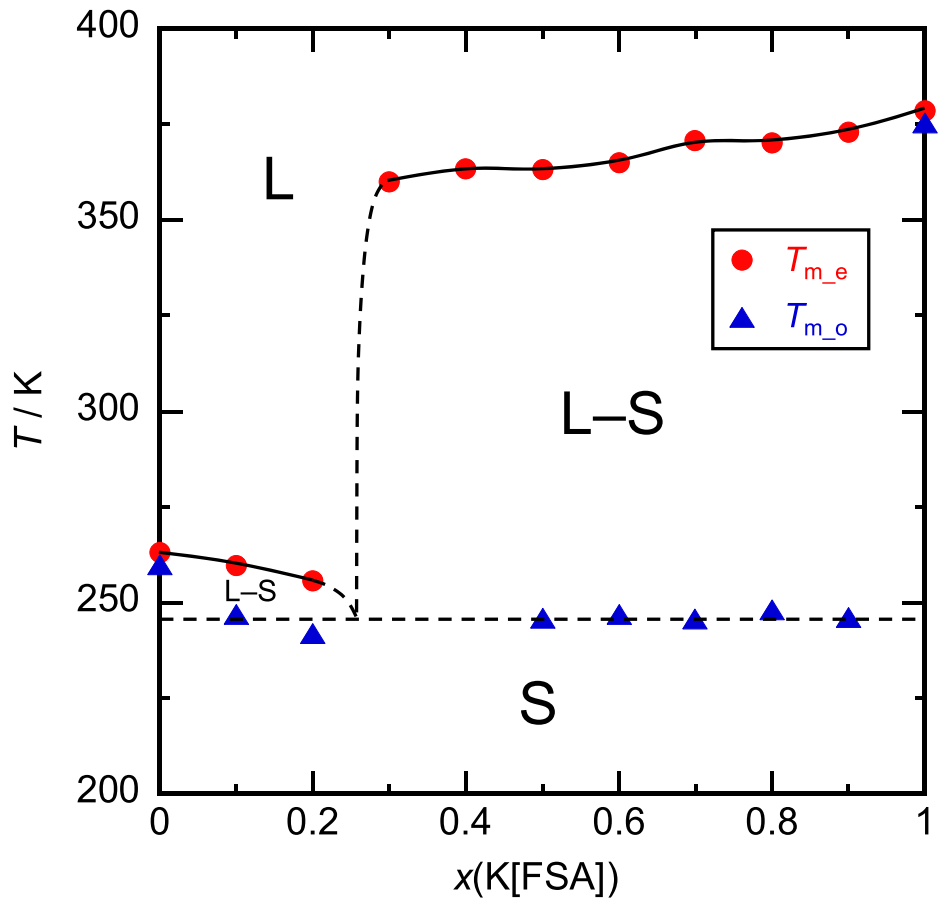

Fig. 1 Phase diagram of the K[FSA]–[C_2C_1im][FSA] system ($0 \leq x$(K[FSA]) ≤ 1; x(K[FSA]): molar fraction of M[FSA]). T_{m_o}: onset temperatures of melting, T_{m_e}: end temperatures of melting. L: liquid region, L–S: liquid–solid coexistence region, S: solid region.

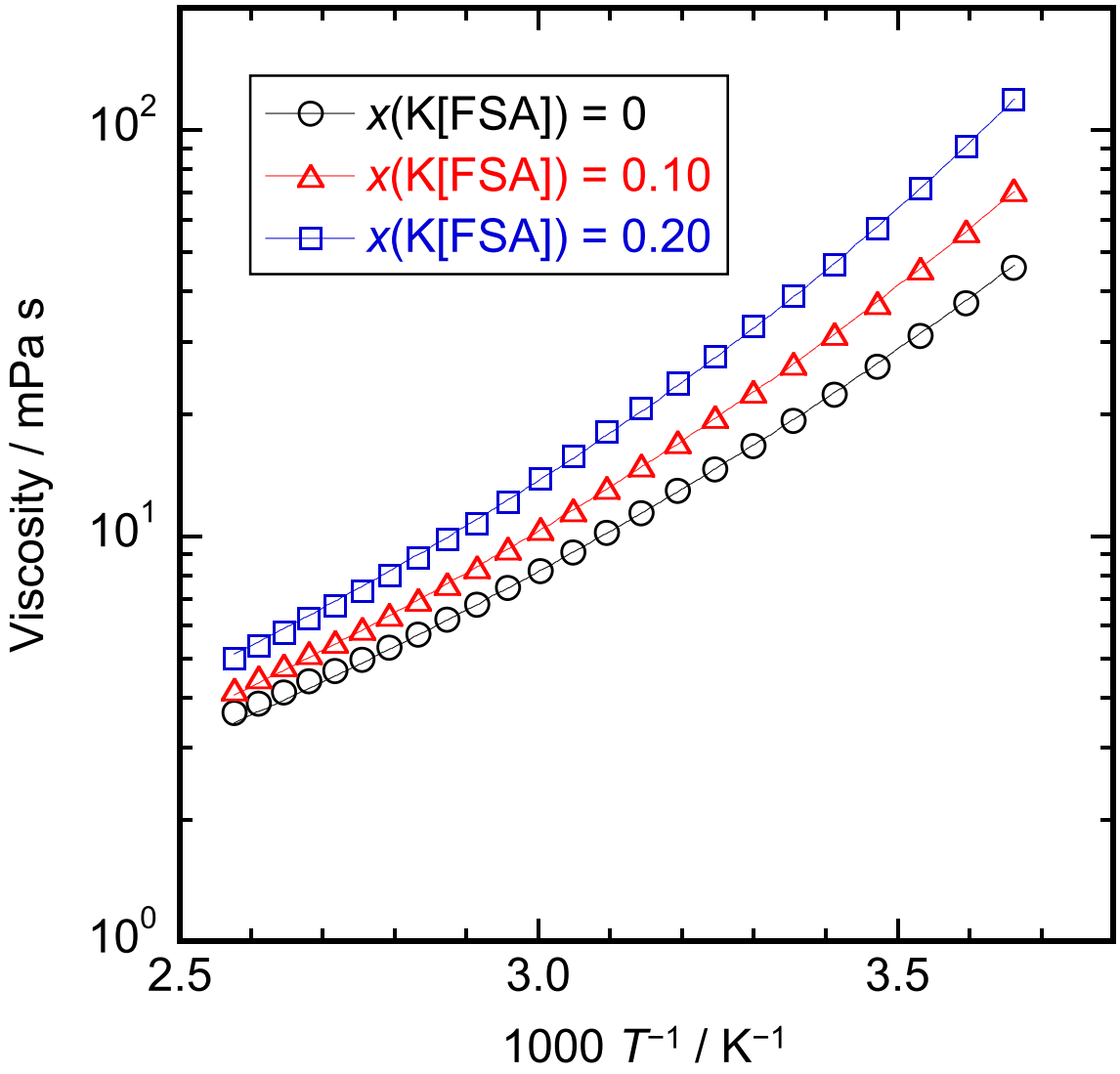

Fig. 2 Arrhenius plots of viscosity for K[FSA]–[C_2C_1im][FSA] (molar fraction of K[FSA]: x(K[FSA] = 0, 0.10, 0.20) ionic liquids. VTF fitting results for all compositions are also provided as solid lines.

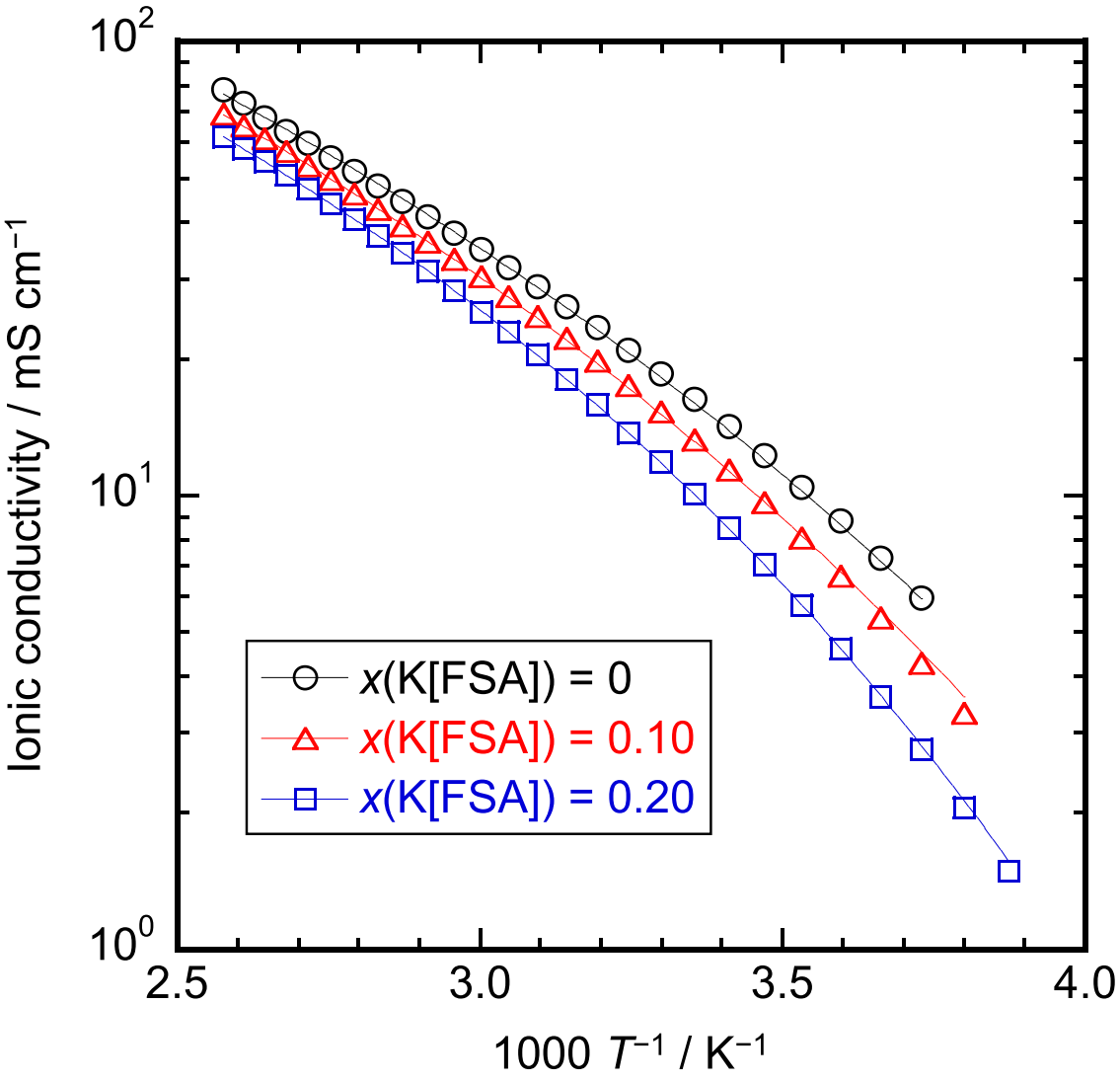

Fig. 3 Arrhenius plots of ionic conductivity for K[FSA]–[C_2C_1im][FSA] (molar fraction of K[FSA]: x(K[FSA] = 0, 0.10, 0.20) ionic liquids. VTF fitting results for all compositions are also provided as solid lines.

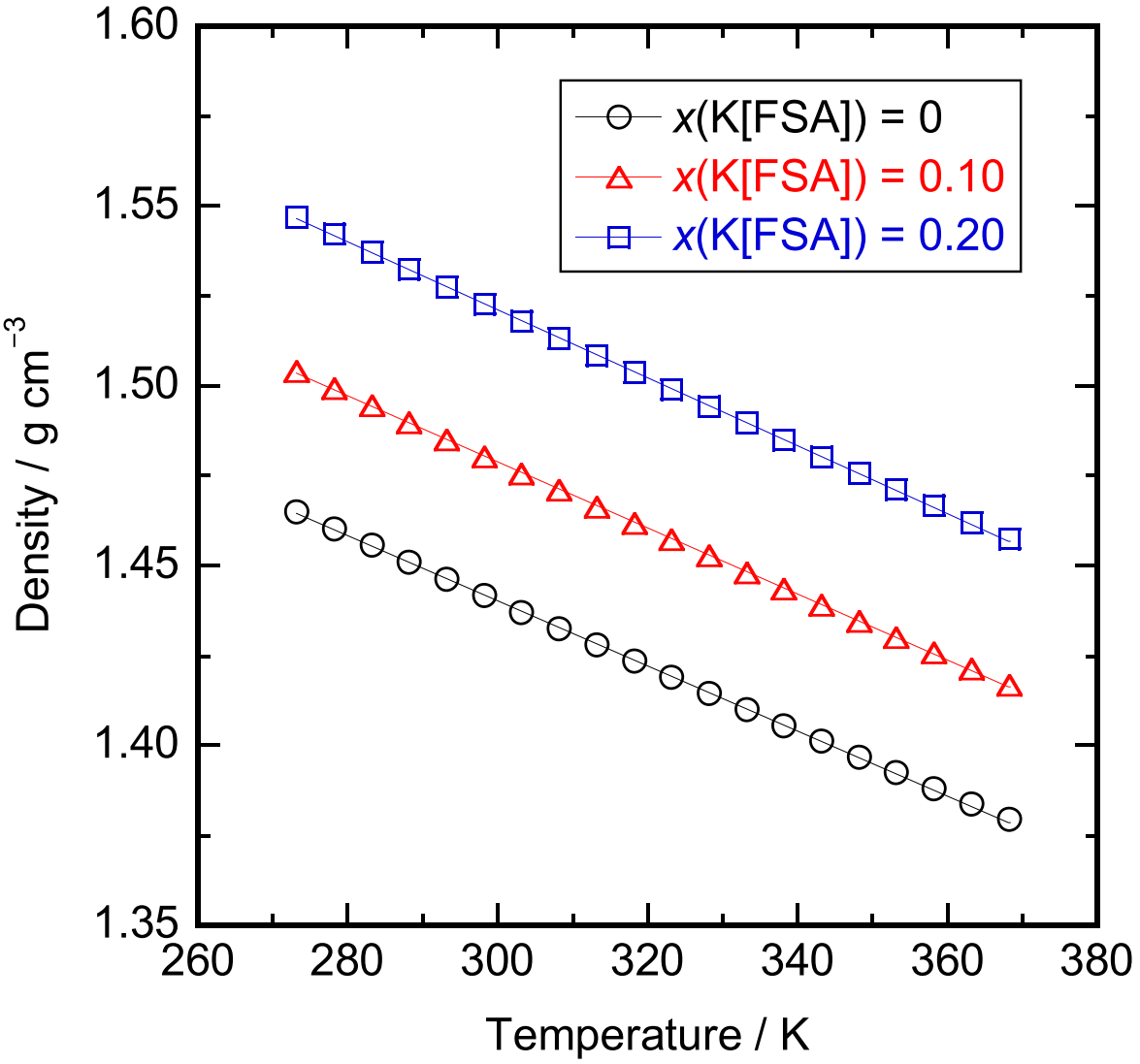

Fig. 4 Density plots of K[FSA]–[C_2C_1im][FSA] (molar fraction of K[FSA]: x(K[FSA] = 0, 0.10, 0.20) ionic liquids. Linear fitting results for all compositions are also provided as solid lines.

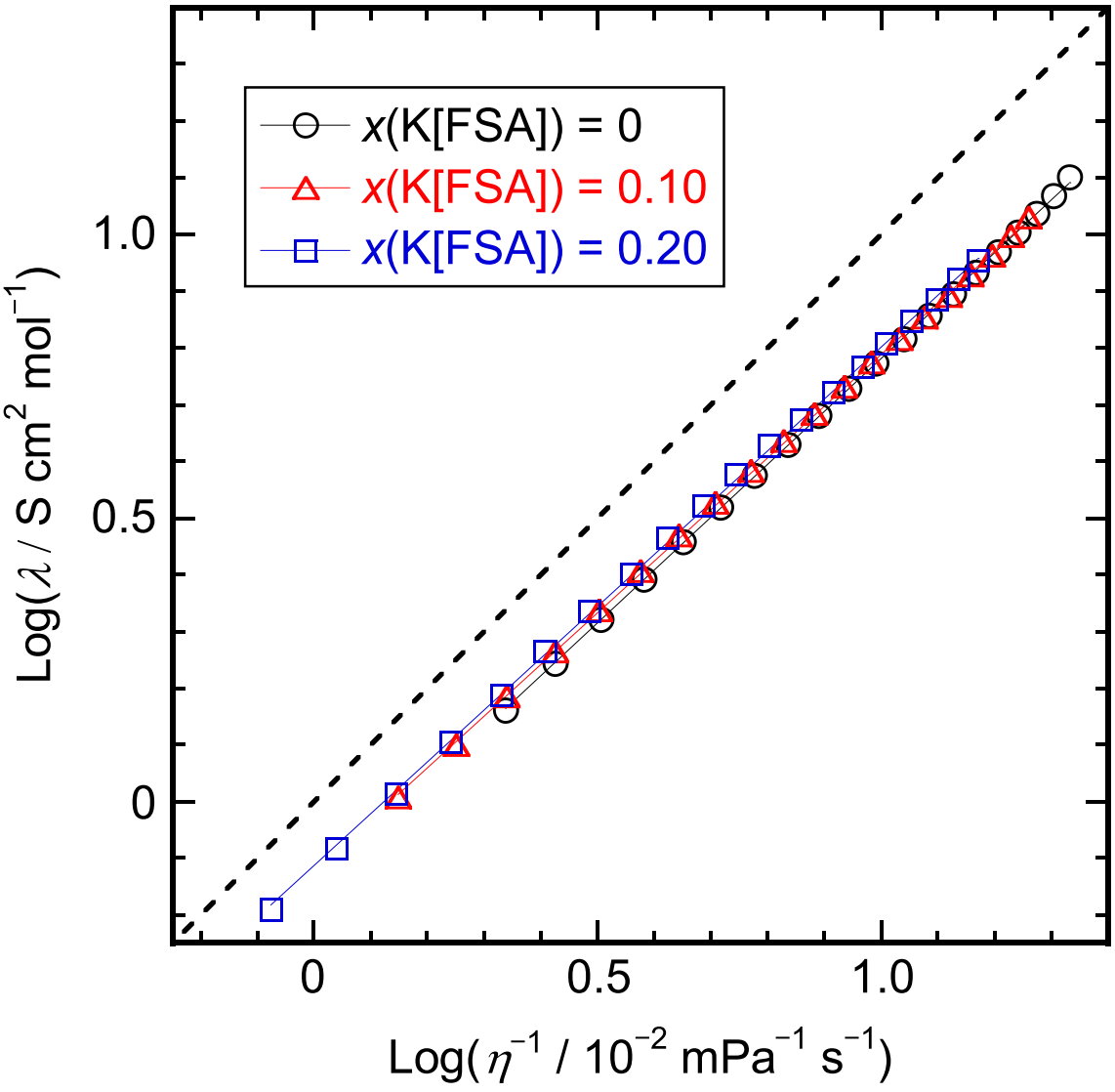

Fig. 5 Walden plots of K[FSA]–[C_2C_1im][FSA] (molar fraction of K[FSA]: x(K[FSA] = 0, 0.10, 0.20) ionic liquids. λ: molar conductivity, η: viscosity. Ideal KCl line is indicated by the broken line, and linear fitting results for all compositions are also provided as solid lines.

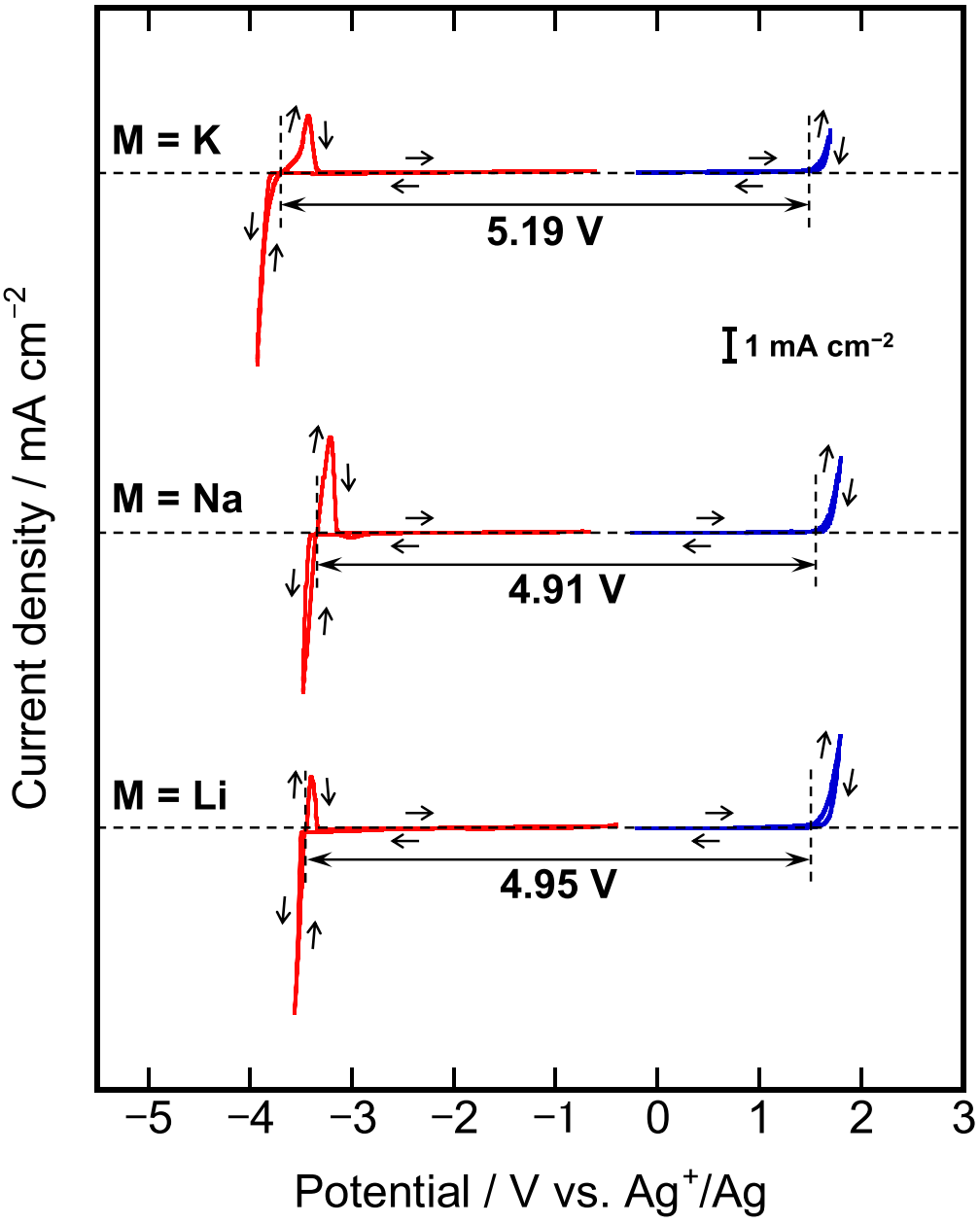

Fig. 6 Cyclic voltammograms of M[FSA]–[C_2C_1im][FSA] (molar fraction of M[FSA]: x(M[FSA]) = 0.20; M = K, Na, Li) ionic liquids at 298 K. Working electrodes: copper disk (negative potential region, red trace), glassy carbon disk (positive potential region, blue trace). Scan rate: 5 mV s^{-1}. Cycle number: 2nd (copper), 1st (glassy carbon). The cathodic and anodic limit potentials of each electrolyte are indicated by vertical dashed lines. Zero current density in each electrolyte is shown as a horizontal dashed line.

Supporting Information

Highly Conductive Ionic Liquid Electrolytes for Potassium-Ion Batteries

Takayuki Yamamoto,* Ryohei Matsubara and Toshiyuki Nohira

Institute of Advanced Energy, Kyoto University, Uji 611-0011, Japan

Corresponding Author

*E-mail: yamamoto.takayuki.2w@kyoto-u.ac.jp, Tel: +81-774-38-3498, Fax: +81-774-38-3499.

Table S1 The onset temperatures of melting (T_{m_o}; K) and the end temperatures of melting (T_{m_e}; K) in DSC measurements for the K[FSA]–[C_2C_1im][FSA] system at 101.3 kPa.[a]

x(K[FSA])[b]	T_{m_o}[c] /K	T_{m_e}[d] / K
0	260	263
0.10	247	260
0.20	242	256
0.30	n.d.	360
0.40	n.d.	364
0.50	246	363
0.60	247	365
0.70	246	371
0.80	248	370
0.90	246	373
1	376	379

Expanded uncertainties (U) are as follows: [a]$U(p)$ = 10 kPa, (0.95 level of confidence); p: pressure. [b]$U(x(\text{K[FSA]}))$ = 0.002 (except for x(K[FSA]) = 0 and 1), (0.95 level of confidence). [c]$U(T_{m\_o})$ = 1 K, (0.95 level of confidence). [d]$U(T_{m\_e})$ = 1 K, (0.95 level of confidence).

Table S2 Molar concentrations ($C(K^+)$; mol dm^{-3}) of K^+ cation and their fitting parameters for the K[FSA]–[C_2C_1im][FSA] (x(K[FSA]) = 0, 0.10, 0.20) ionic liquids at 101.3 kPa.[a]

T [b] / K	$C(K^+)$ [c] / mol dm^{-3}	
	x(K[FSA]) [d]	
	0.10	0.20
273	$0.529_4 \pm 0.0005$	$1.11_7 \pm 0.001$
278	$0.527_7 \pm 0.0005$	$1.11_4 \pm 0.001$
283	$0.526_0 \pm 0.0005$	$1.11_0 \pm 0.001$
288	$0.524_4 \pm 0.0005$	$1.10_7 \pm 0.001$
293	$0.522_7 \pm 0.0005$	$1.10_3 \pm 0.001$
298	$0.521_0 \pm 0.0005$	$1.10_0 \pm 0.001$
303	$0.519_4 \pm 0.0005$	$1.09_6 \pm 0.001$
308	$0.517_8 \pm 0.0005$	$1.09_3 \pm 0.001$
313	$0.516_1 \pm 0.0005$	$1.09_0 \pm 0.001$
318	$0.514_5 \pm 0.0005$	$1.08_6 \pm 0.001$
323	$0.512_9 \pm 0.0005$	$1.08_3 \pm 0.001$
328	$0.511_3 \pm 0.0005$	$1.07_9 \pm 0.001$
333	$0.509_7 \pm 0.0005$	$1.07_6 \pm 0.001$
338	$0.508_1 \pm 0.0005$	$1.07_3 \pm 0.001$
343	$0.506_5 \pm 0.0005$	$1.06_9 \pm 0.001$
348	$0.505_0 \pm 0.0005$	$1.06_6 \pm 0.001$
353	$0.503_4 \pm 0.0005$	$1.06_3 \pm 0.001$
358	$0.501_8 \pm 0.0005$	$1.05_9 \pm 0.001$
363	$0.500_2 \pm 0.0005$	$1.05_6 \pm 0.001$
368	$0.498_7 \pm 0.0005$	$1.05_3 \pm 0.001$
$A_C \times 10^4$ *	-3.22_9	-6.79_8
B_C *	0.617_4	1.30_3
R^2 **	0.9998_5	0.9998_6

*Molar concentration values were fitted by the following equation: $C(K^+) = A_C T + B_C$

**R^2: coefficient of determination

Expanded uncertainties (U) are as follows: [a]$U(p)$ = 10 kPa, (0.95 level of confidence); p: pressure. [b]$U(T)$ = 0.1 K, (0.95 level of confidence). [c]$C(K^+) \pm U(C(K^+))$, (0.95 level of confidence). [d]$U(x(\text{K[FSA]}))$ = 0.002 (x(K[FSA]) = 0.10 and 0.20), (0.95 level of confidence).

Table S3 VTF parameters and $1-R^2$ values (R^2: coefficient of determination) of VTF fitting of viscosity and ionic conductivity for K[FSA]–[C_2C_1im][FSA] ionic liquids (x(K[FSA]) = 0, 0.10, 0.20).

x(K[FSA])	Viscosity				Ionic conductivity			
	$A_\eta \times 10^3$ / mPa s $K^{-1/2}$	B_η / K	$T_{0\eta}$ / K	$(1-R^2) \times 10^4$	$A_\sigma \times 10^{-4}$ / mS cm^{-1} $K^{1/2}$	B_σ / K	$T_{0\sigma}$ / K	$(1-R^2) \times 10^4$
0	5.33	910	128	3.7	3.88	850	126	5.7
0.10	5.36	925	135	0.69	3.77	854	131	0.91
0.20	7.56	840	151	0.62	2.83	740	153	0.09

Table S4 Summary of α and C' (= $\log(\lambda\eta^\alpha)$) parameters for the Walden plots for K[FSA]–[Ocat][FSA] (Ocat = C_2C_1im, C_3C_1pyrr) ionic liquids.

IL	x(K[FSA])	α	C'
K[FSA]–[C_2C_1im][FSA]	0	0.933	−0.152
	0.10	0.911	−0.122
	0.20	0.915	−0.113
K[FSA]–[C_3C_1pyrr][FSA][1]	0	0.911	−0.073
	0.10	0.915	−0.083
	0.20	0.917	−0.107

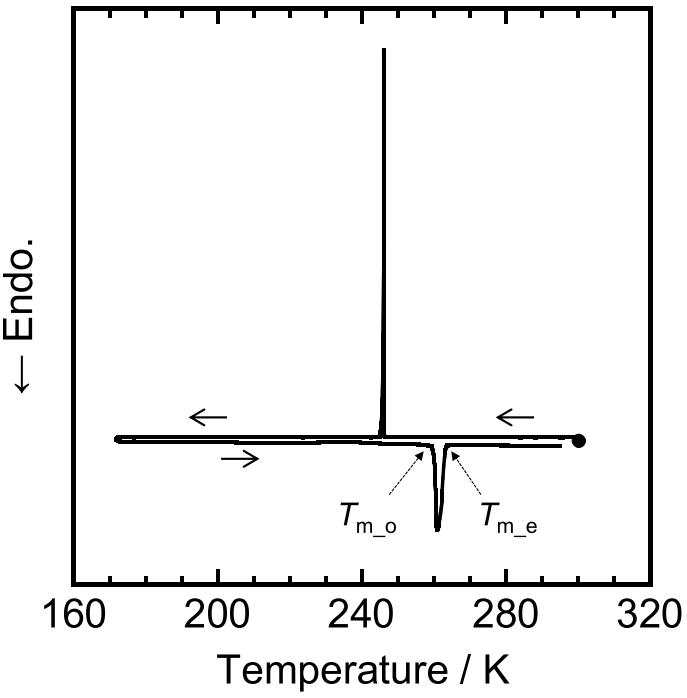

Fig. S1 A DSC curve for $[C_2C_1im][FSA]$. Scan rate: 2 K min^{-1}.

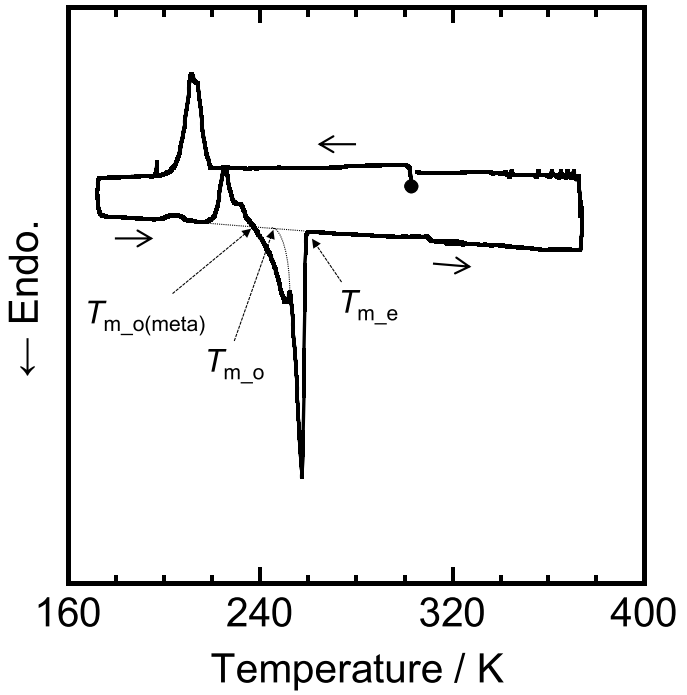

Fig. S2 A DSC curve for K[FSA]–$[C_2C_1im][FSA]$ (x(K[FSA]) = 0.10). Scan rate: 2 K min^{-1}. $T_{m\_o(meta)}$: an onset temperature of melting for a metastable phase.

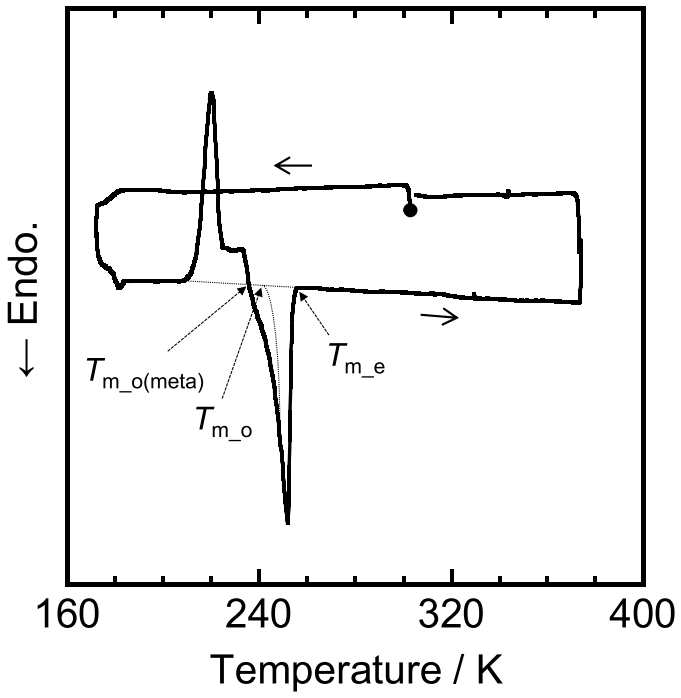

Fig. S3 A DSC curve for K[FSA]–[C_2C_1im][FSA] (x(K[FSA]) = 0.20). Scan rate: 2 K min^{-1}.

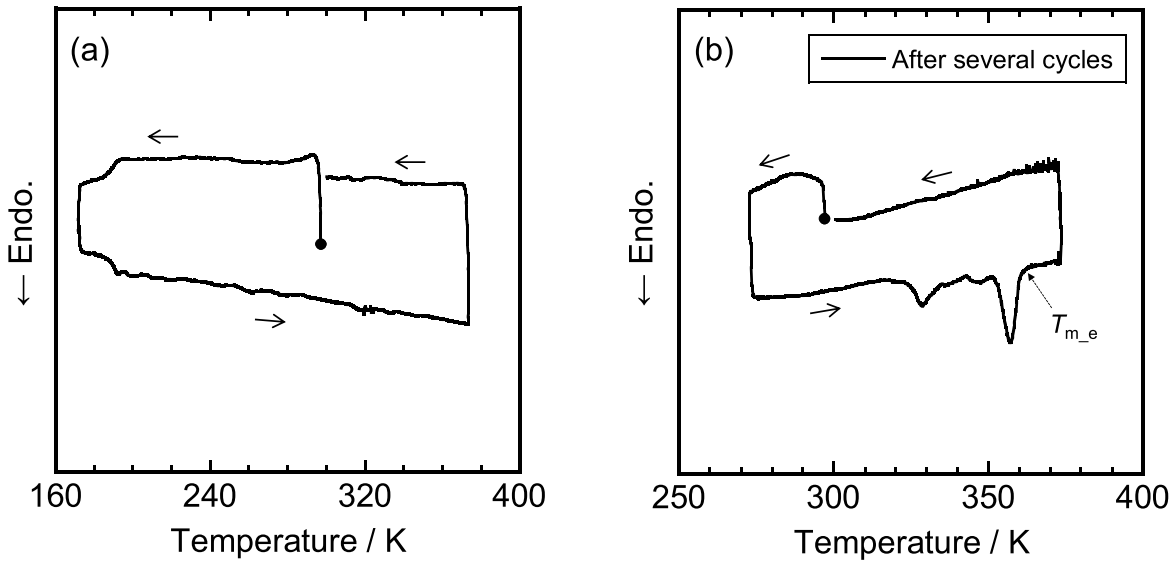

Fig. S4 DSC curves for K[FSA]–[C_2C_1im][FSA] (x(K[FSA]) = 0.30) (a) at a certain cycle and (b) after several cycles of (a). Sample: Scan rate: 2 K min^{-1}.

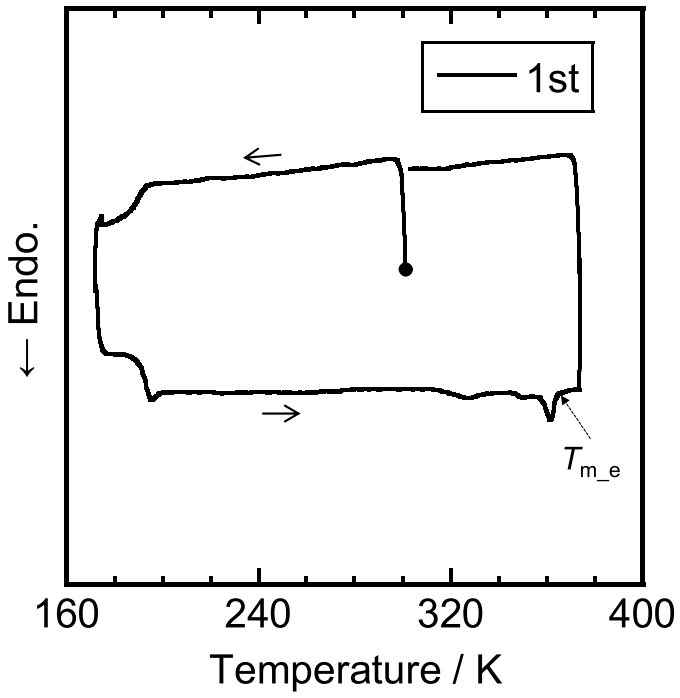

Fig. S5 A DSC curve for K[FSA]–[C_2C_1im][FSA] (x(K[FSA]) = 0.40). Scan rate: 2 K min^{-1}.

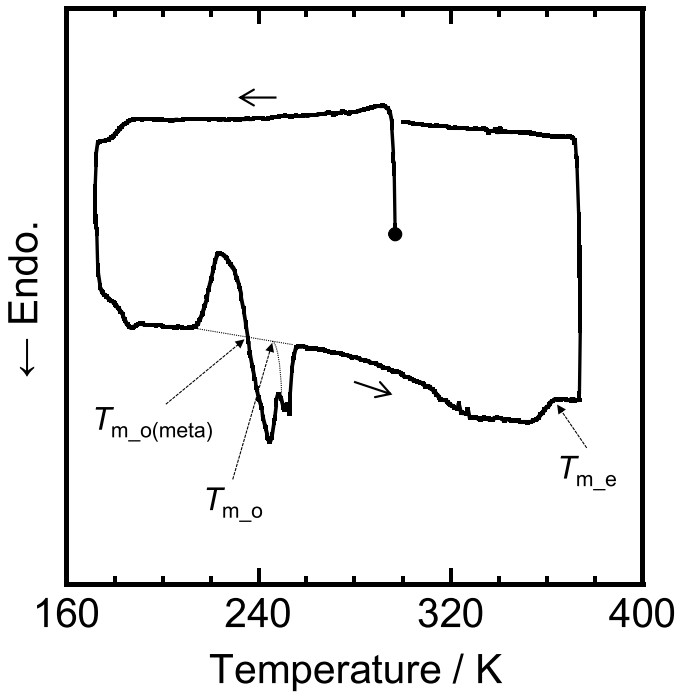

Fig. S6 A DSC curve for K[FSA]–[C_2C_1im][FSA] (x(K[FSA]) = 0.50). Scan rate: 2 K min^{-1}.

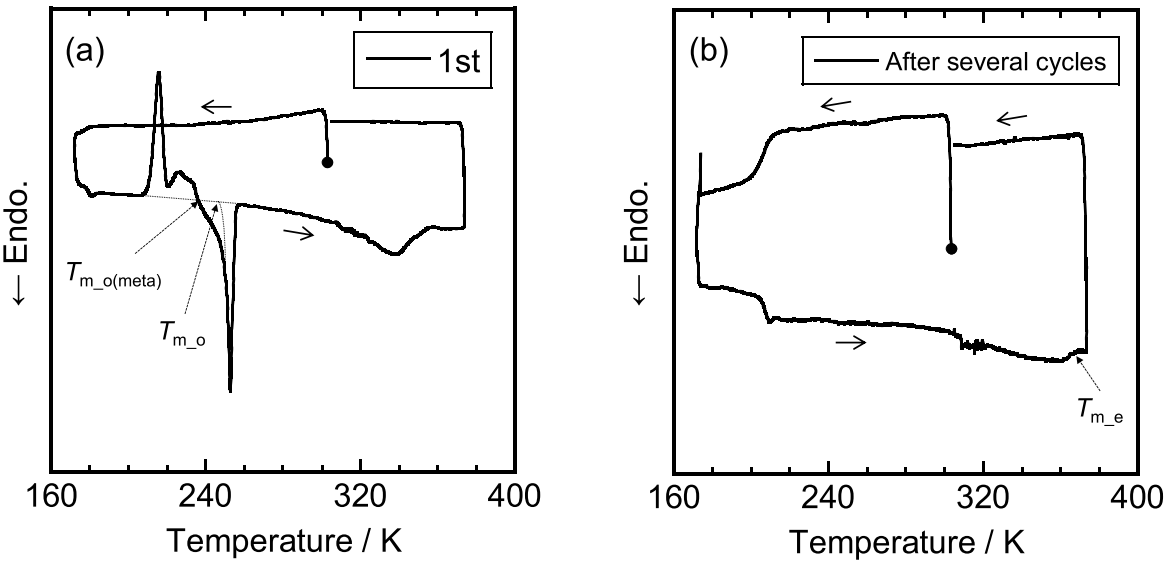

Fig. S7 DSC curves for K[FSA]–[C_2C_1im][FSA] (x(K[FSA]) = 0.60) (a) at 1st cycle and (b) after several cycles of (a). Scan rate: 2 K min^{-1}.

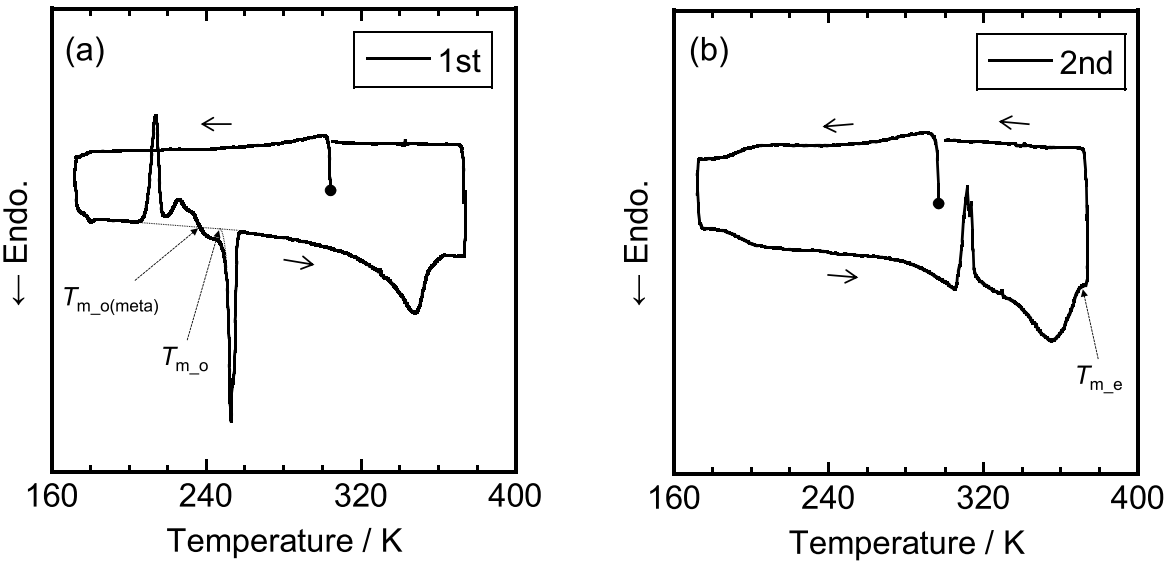

Fig. S8 DSC curves for K[FSA]–[C_2C_1im][FSA] (x(K[FSA]) = 0.70) (a) at 1st cycle and (b) 2nd cycles. Scan rate: 2 K min^{-1}.

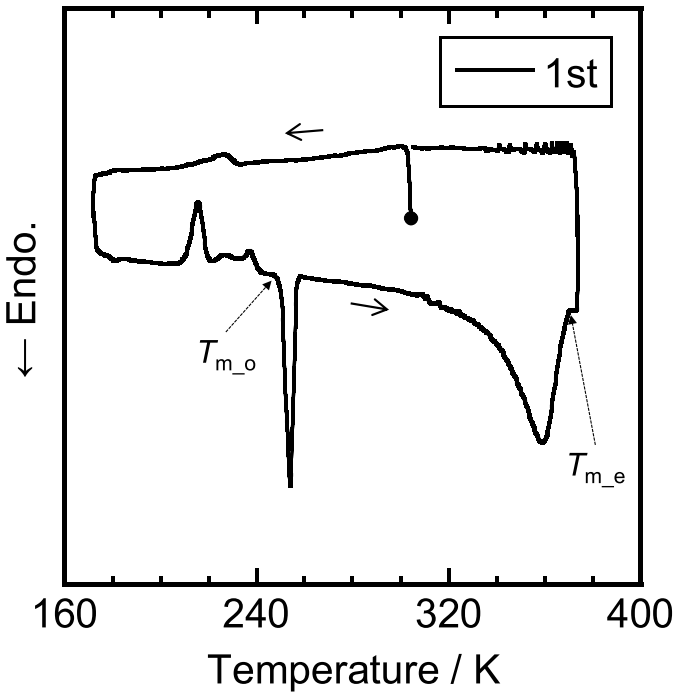

Fig. S9 A DSC curve for K[FSA]–[C_2C_1im][FSA] (x(K[FSA]) = 0.80). Scan rate: 2 K min^{-1}.

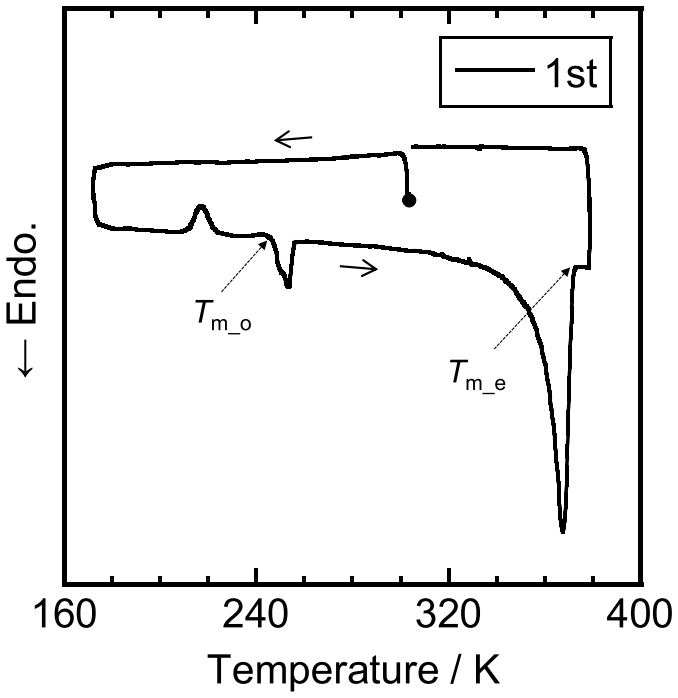

Fig. S10 A DSC curve for K[FSA]–[C_2C_1im][FSA] (x(K[FSA]) = 0.90). Scan rate: 2 K min^{-1}.

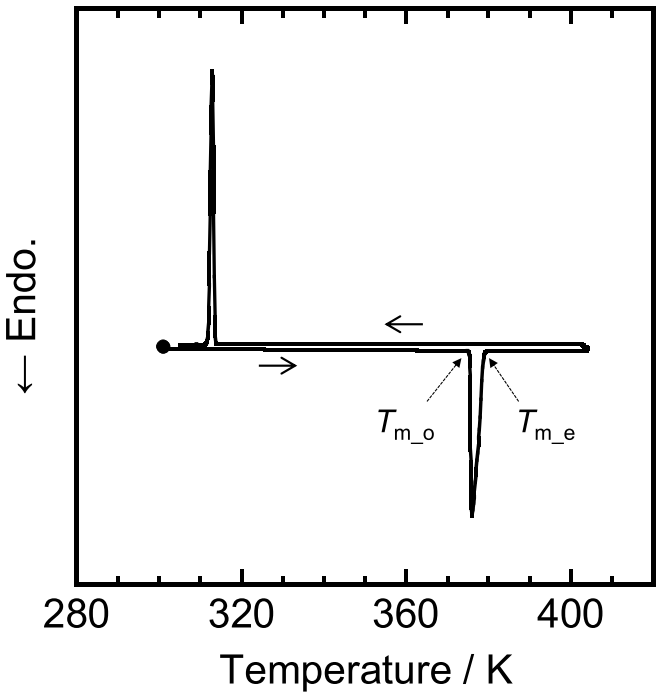

Fig. S11 A DSC curve for K[FSA]. Scan rate: 2 K min^{-1}.

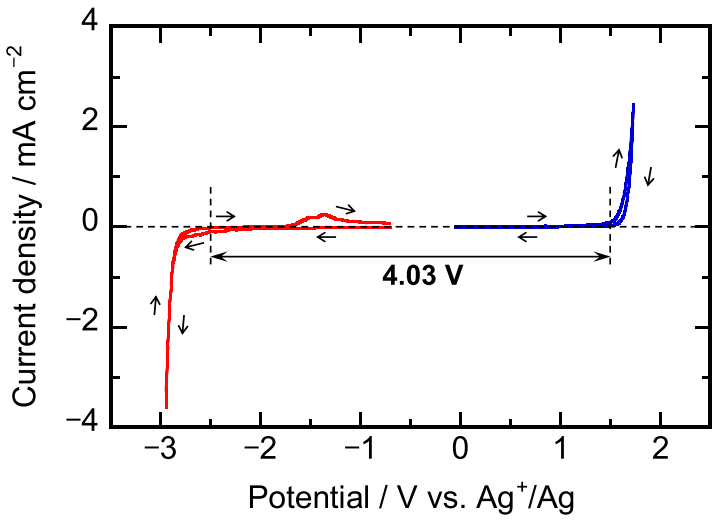

Fig. S12 Cyclic voltammograms of [C_2C_1im][FSA] at 298 K. Working electrodes: copper disk (negative potential region) and glassy carbon disk (positive potential region). Scan rate: 5 mV s^{-1}. Cycle number: 1st. Cathode and anode limits are indicated by vertical dashed lines.

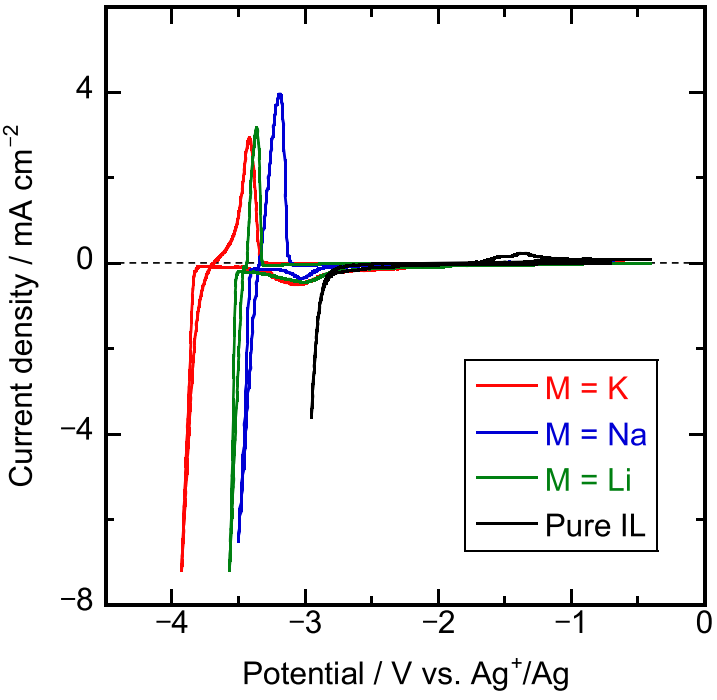

Fig. S13 Comparison of the initial cyclic voltammograms between M[FSA]–[C_2C_1im][FSA] (x(M[FSA]) = 0.20; M = K, Na, Li) and [C_2C_1im][FSA] (Pure IL) ionic liquids at 298 K. Working electrode: copper disk. Scan rate: 5 mV s^{-1}. Cycle number: 1st.

■ REFERENCE

(1) T. Yamamoto, K. Matsumoto, R. Hagiwara and T. Nohira, *J. Phys. Chem. C*, 2017, **121**, 18450–18458.